Influence of Shear on the Templated Crystallization of Poly(butylene terephthalate)/Single Wall Carbon Nanotube Nanocomposites

M. C. García-Gutiérrez,† J. J. Hernández,† A. Nogales,† P. Panine,‡ D. R. Rueda,† and T. A. Ezquerra*,†

Instituto de Estructura de la Materia, CSIC, Serrano 119, 28006 Madrid, Spain, and European Synchrotron Radiation Facility (ESRF), BP 220, F-38043 Grenoble Cedex, France

Received June 19, 2007; Revised Manuscript Received November 2, 2007

ABSTRACT: The templating effect due to single wall carbon nanotubes (SWCNT) and shear on polymer crystallization has been studied in films of nanocomposites based on poly(butylene terephthalate) (PBT). With the use of a rheometer, a step shear was applied to the molten polymer. After shear cessation, the sample was immediately cooled down to the crystallization temperature. Crystalline development, in real time, was investigated by small-angle X-ray scattering (SAXS) with a synchrotron radiation beam parallel to the film. SWCNT bundles template polymer lamellae to grow perpendicular to the SWCNT surfaces in a shish-kebab fashion even under quiescent conditions. Because of the power of SWCNT as nucleating agents, the shear rate has a minor effect on the crystallization kinetics. However, the fraction of oriented material increases significantly with shear rate. The results indicate that SWCNT act as nuclei stabilizers, providing surfaces which favor polymer crystallization.

1. Introduction

Since the discovery of carbon nanotubes by Iijima in the early nineties,[1] the scientific activities in this field have followed an exponential increase due to the remarkable physical properties of this novel form of carbon.[1−5] Single wall carbon nanotubes (SWCNT) are shown to be promising reinforcing elements, with Young's moduli in the TeraPascal (TPa) range, for a new generation of nanocomposite materials.[4−6] A typical SWCNT sample consists of micrometer-size aggregates, frequently referred to as bundles or ropes. Within the ropes, single nanotubes self-assemble into a two-dimensional hexagonal close-packed lattice.[7] A homogenization of the nanotubes down to the nanometer level is required upon mixing with a polymeric matrix. This can be attempted by using different procedures including compounding, sonication, and shear among others.[4−6] In general, typical polymeric nanocomposite processing involves solidification, either by crystallization or by vitrification, from a molten state which is distorted by a combination of shear and elongational flow fields. The effect of processing induced flow fields on the nanostructure of polymers and nanocomposites is crucial because of the profound impact on their physical properties.[4,5,8−11] The effect of shear fields, mimicking those used in industrial processing on the structure of SWCNT polymer nanocomposites remains almost untreated until now. Recent experiments have shown that, additionally to the nucleating effect of SWCNT,[12] this type of carbon nanotube is very efficient in templating oriented polymer crystal growth.[13−17] In these studies, different processing routes have been explored including injection moulding,[14,17] fiber spinning,[15] and crystallization from solution.[13] In these works it has been shown that the SWCNT surface imposes to polymer crystals a growth direction perpendicular to the nanotube longitudinal main axis. It is known that both injection moulding and fiber spinning involve a complex thermal and flow history to the sample. Thus, it is difficult to separate the effect of flow field from thermal gradients on polymer crystallization. However, by using either a rheometer or a shear cell, thermal and flow effects can be separated. This can be accomplished by choosing the appropriate combination of shear strain, shear rate, and temperature.[8−11] Until now, as far as X-ray scattering is concerned, most of the shear-induced crystallization studies have been carried out by means of rotating parallel plate equipment. Here, the X-ray beam reaches the sample perpendicular to the flat surface of the rotating plates.[8−11] This disposition is quite appropriate because it guarantees a nearly constant shear rate on the explored sample volume. However, upon dealing with SWCNT/polymer nanocomposites, the nanotubes may tend to adopt orientations in which their main axes are located preferentially parallel to the surface plates. This effect is mainly due to the high aspect ratio of SWCNT. In this case, an X-ray beam parallel to the flat surface of the rotating plates can be advantageous because orientations parallel to the rotating plates can be probed. The aim of this work is to study the crystallization of nanocomposites based on SWCNT under the controlled shear fields provided by a rheometer[18] in which the X-ray beam reaches the sample holder parallel to the film (Figure 1). Our main objective is to advance in answering two basic questions: (1) Under which conditions do SWCNT template an oriented crystallization? and (2) How can shear rate be used to control templating?. In order to accomplish both tasks, a matrix of poly(butylene terephthalate) (PBT) was selected due to the extensive body of previous shear-induced crystallization on this polymer.[10] In addition, PBT/SWCNT nanocomposites can be prepared by "in situ" polymerization rendering rather good SWCNT dispersions.[19]

2. Experimental Section

2.1. Polymer Samples. For this study, several nanocomposite samples of poly(butylene terephthalate) (PBT) ($M_w \approx 15\,000$ g/mol, melting temperature $T_m = 225.3$ °C) with different amounts of oxidized single wall carbon nanotubes (SWCNT) (from CNI Technology Co., Texas, synthesized by using the HiPco method) were prepared. The Raman spectra show that the investigated SWCNT consist of different diameter populations[20] ranging from about 0.6 to 1.4 nm. The PBT/SWCNT nanocomposite preparation scheme follows an "in situ" polymerization strategy.[19] The SWCNT were first dispersed by ultrasonication and high-speed stirring in

* To whom correspondence should be addressed.
† Instituto de Estructura de la Materia, CSIC.
‡ European Synchrotron Radiation Facility (ESRF).

10.1021/ma0713512 CCC: $40.75
Published on Web 12/29/2007

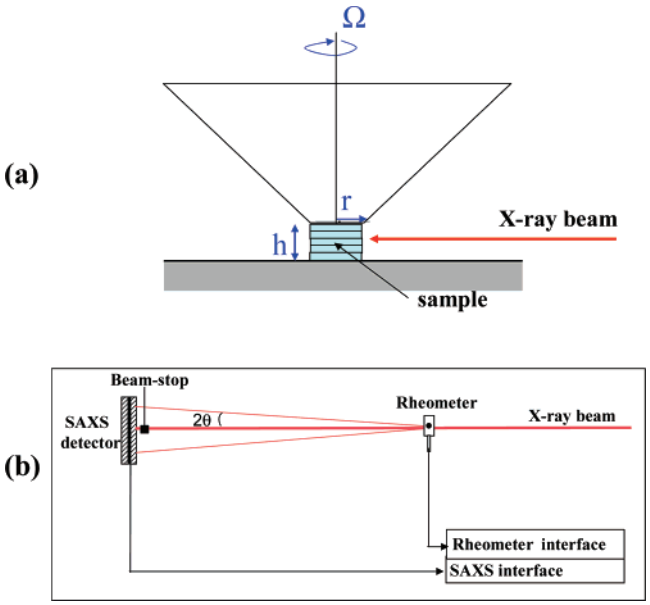

Figure 1. (a) Scheme of the sample holder: the sample (consisting of stacked films) fills the gap of height h, between a truncated cone of radius r, and the substrate plate. The cone rotates with an angular speed, Ω. (b) Schematic view of the experimental setup for Rheo-SAXS experiments. 2θ is the scattering angle.

1,4-butanediol (BASF, Germany). Polycondensation was then accomplished by transesterification with dimethyl terephthalate (Elana S.A., Torun, Poland) in an acid-resistant steel reactor.[19] The nanocomposite was extruded from the reactor by compressed nitrogen. Subsequently, it was pelletized and injection molded with a Baby Plast, model 6/10 (Cronoplast S.L. Comp.) machine into long pieces with a rectangular cross section of 2 × 4 mm^2. The injection molding parameters were injection pressure 25 bar, melt temperature 240−250 °C, mold temperature 40 °C, hold time 6 s, and cool time 20 s. Nanocomposite films of about 0.1 mm thickness were obtained by compression molding at 240 °C for 2 min and subsequently quenched under constant pressure at a cooling rate of ∼300 °C min^{-1}.

2.2. Rheo-SAXS Measurements. Small-angle X-ray scattering (SAXS) measurements were performed at the ID2 beam line of the European Synchrotron Radiation Facility (ESRF) in Grenoble, France. Shear was applied to the sample by using a modified RS300 (HAAKE) rheometer.[18] The commercial rheometer was modified to accommodate a truncated cone of $r = 3$ mm in diameter at the end of the inner cylinder, as schematically depicted in Figure 1a. The gap set to $h = 0.6$ mm was filled with about six films piled up and parallel to the incident X-ray beam. Under these conditions, the maximum shear rate applied to the sample is given by $\dot{\gamma}_m^\circ = (r/h)\Omega$, where Ω is the angular speed. The overall setup provides a temperature stability of the sample better than 0.05 °C. The rheometer was located in the X-ray beam path, as schematically illustrated in Figure 1b. The synchrotron radiation was monochromatized to provide an X-ray wavelength of $\lambda = 0.1$ nm. SAXS intensity was recorded by a two-dimensional CCD camera (FReLoN Kodak CCD, with an input area of 100 × 100 mm^2). The sample to detector distance was fixed to 2640 mm. Typical beam size at the sample position is 0.1 × 0.1 mm^2. An initial data reduction is accomplished in order to correct for detector distortion and to normalize to the intensity of the primary beam. Figure 2 describes schematically the type of shear experiments we accomplished in this study. A step shear was applied to the molten polymer for a certain time at a temperature higher than its melting temperature. In the present study, we selected $T = 240$ °C which is well above the melting temperature of PBT. After cessation of the shear, the sample was immediately cooled down to the crystallization temperature, T_c, at a cooling rate of 10 °C/min. Crystallization was followed by measuring the SAXS patterns as a function of time. By this procedure, the flow and the crystallization processes can

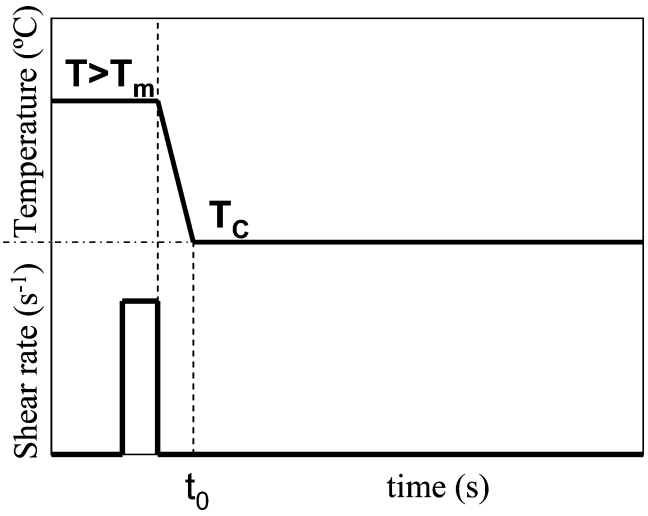

Figure 2. Schematic description of the step shear experiments. After reaching a temperature higher than the melting temperature, T_m, the sample is subjected to a step shear for a certain time. After shear cessation, the sample is cooled down to the crystallization temperature, T_c.

be effectively separated.[21] Different maximum shear rates, $\dot{\gamma}_m^\circ$, of 0, 5, 10, and 20 s^{-1} were applied for different times in order to obtain a maximum constant strain of 2000%. Two-dimensional SAXS images were taken immediately after the polymer reached T_c. The data acquisition time for each 2D scattering pattern was typically 0.1 s. The time between two consecutive patterns was fixed to be 10 s. An air scattering pattern was also collected. The air scattering pattern was used for background correction of the scattering data. Additionally, a normalization of the scattered intensity was accomplished considering the intensity of the primary beam. Subsequent analysis of the X-ray data was carried out using the corrected and normalized scattering patterns. The crystallization temperature was chosen on the basis of previous shear-induced crystallization experiments in PBT.[10] Here it was shown that, under small supercooling conditions, shear flow accelerates crystallization kinetics but leads to little preferred crystal orientation. The small supercooling temperature region was reported to start for $T_c \geq 203$ °C. Therefore, in this study, a $T_c = 208$ °C was chosen, well located within the small supercooling region. In this way, the possible templating effect of SWCNT in PBT crystallization can be better investigated.

2.3. Atomic Force Microscopy (AFM). Atomic force microscopy (AFM) was used to visualize the microstructure and morphology of PBT/SWCNT nanocomposites. We used a Nanoscope IIIA Multimode from Vecco operating in the tapping mode. The surface of the sheared samples was examined ex situ. Additional samples were prepared by spin coating on a silicon wafer (100) (Wafer World Inc.) from a trifluoracetic acid solution (20 g L^{-1}). A precise volume of 0.1 mL of the polymer solution was instantly dropped by a syringe on a rectangular (about 2 × 2.5 cm^2) silicon substrate centered on a rotating plate at 2380 rpm for 30 s. Samples were stored at room temperature preventing them from acquiring dust.

2.4. Data Analysis. The 2D SAXS patterns were analyzed in order to obtain different magnitudes including the oriented fraction, the Hermans orientation function, and the integrated intensity.

2.4.1. Oriented Fraction. The oriented fraction was obtained empirically on the basis of an experimental strategy developed for PBT,[10] which is schematically described in Figure 3. Basically, a 2D SAXS pattern (Figure 3a) is divided into two quadrants chosen to represent the scattering and centered along the meridian (φ = 0−180°) and the equator (φ = 90−270°), respectively. A cake, represented by the continuous lines in Figure 3a, is defined in each quadrant with a width of $\Delta q = 20$ nm^{-1}, where q is the scattering vector $q = 4\pi\lambda^{-1} \sin\theta$, and 2θ is the scattering angle. The cakes are centered at the q-values corresponding to the maximum scattered intensity. The scattered intensity is radial integrated within the cakes

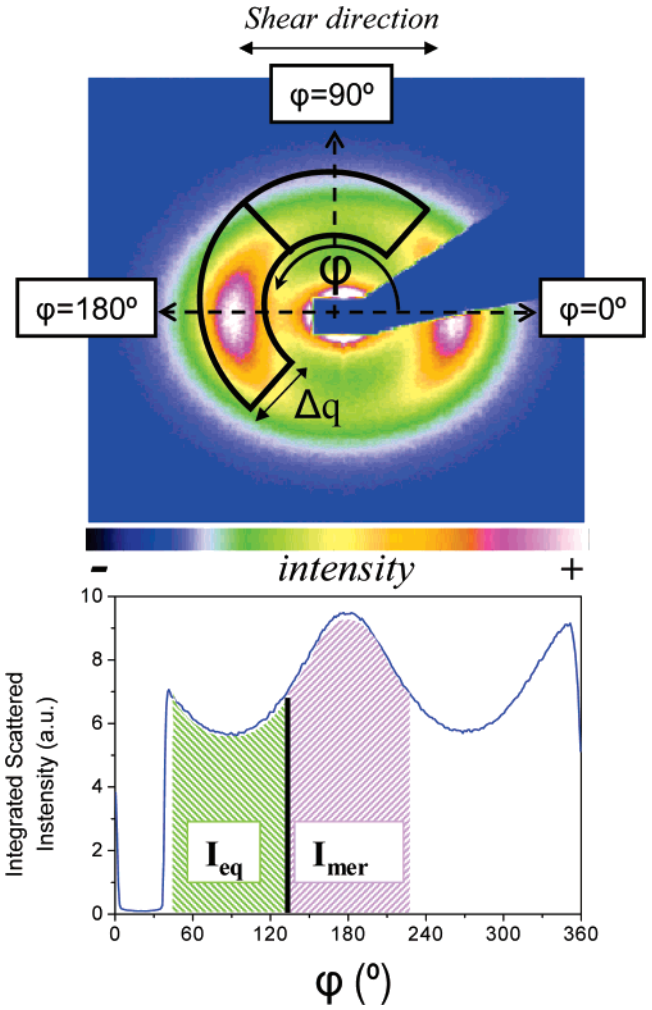

Figure 3. Example of the data analysis strategy used to extract an empirical oriented fraction, Φ, from the two-dimensional SAXS patterns. (a) Two cakes, represented by the continuous lines, are defined in two quadrants centered at the meridian ($\varphi = 180°$) and at the equator ($\varphi = 90°$), respectively. The width of the cakes is $\Delta q = 20$ nm^{-1}, where q is the scattering vector $q = 4\pi\lambda^{-1} \sin\theta$, and 2θ is the scattering angle. The cakes are centered at the q-values corresponding to the maximum scattered intensity. (b) The scattered intensity is first radial integrated within the cakes and represented as a function of the azimuthal angle φ. The shadowed regions represent the magnitudes I_{mer} and I_{eq} for the meridian and equator contributions, respectively. An empirical oriented fraction parameter Φ can be defined from these magnitudes by means of eq 1.

and represented as a function of the azimuthal angle φ (Figure 3b). A second integration in φ can be done in order to define the magnitudes I_{mer} and I_{eq} for the meridian and equator regions, respectively. These two quantities have been represented in Figure 3b by the shadowed regions.

Subsequently, an empirical oriented fraction parameter Φ can be defined by means of

$$\Phi = \frac{I_{mer} - I_{eq}}{I_{mer} + I_{eq}} \tag{1}$$

2.4.2. Orientation Function. The Hermans orientation function is commonly used to estimate the orientation of a sample from the analysis of wide-angle X-ray scattering data. In addition, it has been demonstrated that it is also useful to evaluate the orientation of crystalline lamellae from a SAXS pattern.[22] In this case, the Hermans orientation function f_2 is given by

$$f_2 = \frac{3\langle\cos^2\varphi\rangle - 1}{2} \tag{2}$$

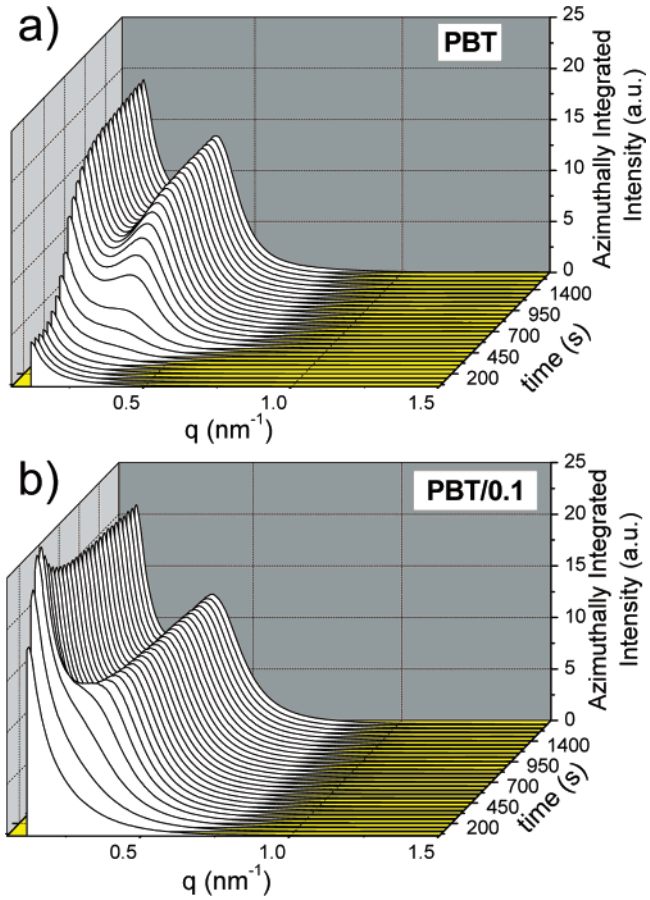

Figure 4. Time evolution of the azimuthally integrated intensity as a function of the q-vector during a crystallization experiment at T_c = 208 °C for: (a) PBT and (b) PBT/0.1 wt % SWCNT nanocomposite after the application of a step shear (shear rate of 10 s^{-1}) at T = 240 °C.

where

$$\langle\cos^2\varphi\rangle = \frac{\sum_{\varphi_i=0}^{90°} I_i \sin\varphi_i \cos^2\varphi_i}{\sum_{\varphi_i=0}^{90°} I_i \sin\varphi_i} \tag{3}$$

with I_i being the scattered intensity at the ith azimuthal angle φ_i. In our case, this calculation was done by azimuthal cake integrations with three cake sizes in order to have an estimation of the error in the values of f_2. The zero position for φ was set at the meridian of the pattern and φ runs anticlockwise (see Figure 3a). Meanwhile, the initial and final angles for the integration were chosen to be $\varphi = 90°$ and $\varphi = 180°$, in order to avoid the shadow of the beam-stop. The f_2 function was normalized by shifting the background to zero. In this case, the orientation function takes the value $f_2 = 1$ when the scattered intensity concentrates on the meridian and $f_2 = -0.5$ when the scattered intensity concentrates on the equator. For an isotropic pattern, a value of $f_2 = 0$ is expected.

2.4.3. Integrated Intensity. The scattering patterns can be azimuthally integrated in order to obtain the one-dimensional (1D) scattering intensity as a function of the scattering vector q. As an example, Figure 4 shows the time evolution of the azimuthally integrated intensity as a function of the q-vector during a crystallization experiment at T_c = 208 °C for PBT (Figure 4a) and for a PBT/0.1 wt % SWCNT nanocomposite (Figure 4b) after the application of a step shear (shear rate of 10 s^{-1}) at T = 240 °C. It is clear that the appearance during crystallization of a peak in intensity whose position, q_{max}, can be used to define the charac-

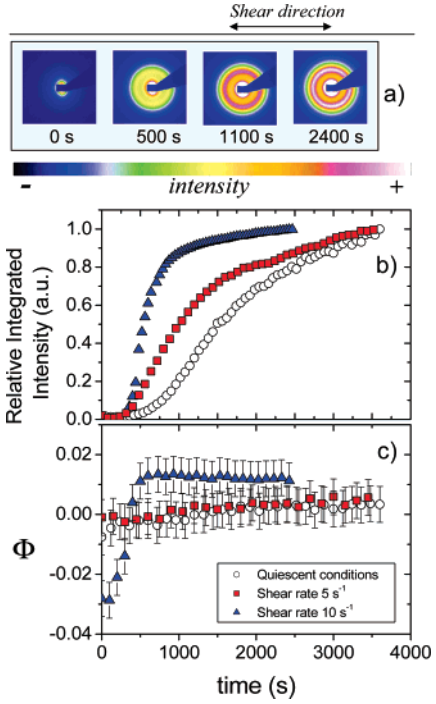

Figure 5. Crystallization of PBT at $T_c = 208$ °C after the application of a step shear at $T = 240$ °C (shear rate of 10 s^{-1}). (a) SAXS patterns as a function of time. (b) Relative integrated SAXS intensity during crystallization as a function of time for different shear rates. (c) Oriented fraction as a function of crystallization time at different shear rates.

teristic long period, L, of the crystalline lamellar stacks by means of the equation $L = 2\pi/q_{max}$. The peaks were fitted to Gaussian curves in order to obtain an accurate value of q_{max}. A further integration in the q-range of the scattered intensity allows one to define the total integrated intensity. This magnitude, represented as a function of time, can be used to characterize the crystallization kinetics. In order to compare different crystallization kinetics, the value at the initial time can be subtracted and the resulting data can be normalized to the value at the end of the crystallization process. The resulting magnitude is sometimes referred to as the relative integrated intensity. The half time of crystallization is defined as the time required to reach one-half of the maximum relative integrated intensity.

3. Results

3.1. Shear-Induced Crystallization of the PBT Matrix. Figure 5a shows a series of 2D SAXS patterns for PBT taken at $T_c = 208$ °C after the application of a step shear (shear rate of 10 s^{-1}) at $T = 240$ °C > T_m. With a start from an amorphous supercooled melt at $t = 0$ s, crystallization takes place with time as revealed by the appearance of an essentially isotropic ring associated to the characteristic long spacing of the lamellar stacks.[10] The appearance of the long spacing is evidenced in the 1D plots shown in Figure 4a. Figure 5b shows the relative integrated SAXS intensity as a function of time for different shear rates. Figure 5c represents the oriented fraction, calculated as described above, as a function of time for the different shear rates investigated. Only for the higher shear rate (10 s^{-1}) a small level of orientation is observed at the end of the crystallization process. The initial negative value of Φ in this case indicates a preferential orientation of the scatterers along the meridional direction. The amount of oriented fraction tends to zero at intermediate times and finally reaches a small positive value. A qualitatively similar behavior has been previously reported for PBT under shear conditions.[10] Here, Li et al. attributed this effect to the initial formation of row nuclei parallel to the flow

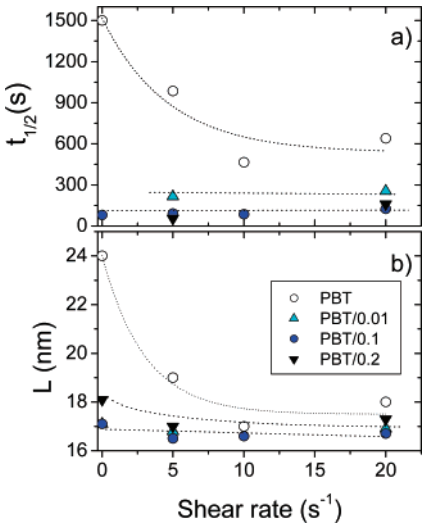

Figure 6. (a) Half time of crystallization and (b) long spacing as a function of shear rate for different SWCNT wt %. $T_c = 208$ °C.

direction. Because of chain relaxation, row nuclei break down into pointlike nuclei leading to a very small oriented fraction. Figure 6a represents the half time of crystallization as a function of shear rate at $T_c = 208$ °C. As expected for PBT, crystallization kinetics tends to become faster as shear rate increases.[10] A slight increase of the half time is observed for a shear rate of 20 s^{-1}. This effect can be due to a possible chain scission mechanism under the present experimental conditions. In qualitative agreement with previous results,[10] long spacing values tend to decrease with increasing shear rate (see Figure 6b, PBT data). For comparative purposes, Figure 6 also includes the results obtained for the nanocomposites to be commented on in the next paragraphs.

3.2. Crystallization of PBT/SWCNT Nanocomposites under Quiescent Conditions. Figure 7a shows the relative integrated SAXS intensity as a function of crystallization time for PBT and for a PBT/0.1 wt % SWCNT nanocomposite under quiescent conditions at $T_c = 208$ °C. As previously reported, even a modest amount of carbon nanotubes produces a strong enhancement of the crystallization kinetics of the polymer matrix. Carbon nanotubes provide nucleation surfaces over which polymer crystals can easily grow.[5,15] However, it is more striking that, as shown in Figure 7b, a significant orientation appears for the nanocomposite even under quiescent conditions. This is revealed by the strongly anisotropic SAXS pattern obtained at the end of the crystallization experiment, as shown in the inserts of Figure 7a. Figure 8 presents in the two first columns the initial, t_0, and final, t_f, SAXS patterns obtained for PBT and for the PBT/0.1 wt % SWCNT nanocomposite. While PBT exhibits almost no orientation features at the end of the crystallization process, the pattern of the nanocomposite shows a significant orientation. For the nanocomposite, the initial pattern at t_0 shows an excess of scattering in the equatorial region. This is characteristic of scatterers oriented parallel to the film surface. However, for the final pattern the scattered intensity concentrates in the meridian region. This indicates the existence of scatterers perpendicular to the film surface. At this point, it is worth mentioning the importance of the film position in the experimental setup (Figure 1). This fact was revealed by SAXS experiments performed in the A2 beam line at Hasylab, Hamburg. Here, a classical geometry was used with the X-ray beam reaching the sample perpendicular to the film (see cartoon on top of Figure 8). Thus, the SAXS pattern of a PBT/0.1 wt % SWCNT nanocomposite obtained with this geometry shows

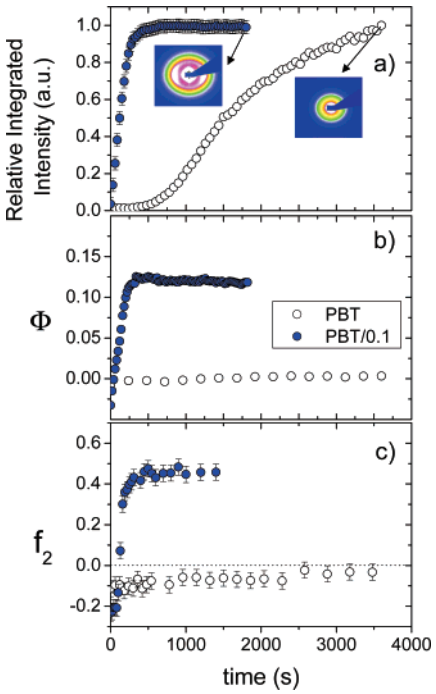

Figure 7. Time dependence of (a) the relative integrated SAXS intensity, (b) the oriented fraction, and (c) the Hermans orientation function for PBT and a PBT/0.1 wt % SWCNT nanocomposite under quiescent conditions at $T_c = 208$ °C. The two images inserted in part a correspond to the SAXS patterns at the end of the crystallization process.

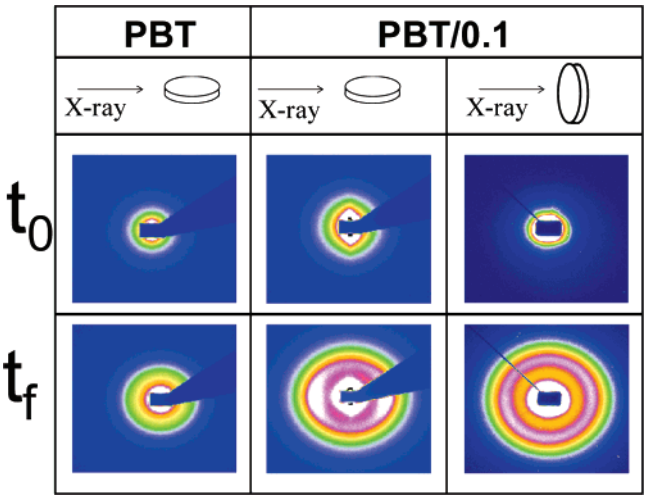

Figure 8. SAXS patterns of PBT and of PBT/0.1 wt % SWCNT nanocomposite for initial, t_0, and final, t_f, times under quiescent crystallization at $T_c = 208$ °C. From left to right, the first two columns show the patterns when the film is parallel to the X-ray beam. The last column shows the patterns for the nanocomposite when the film is perpendicular to the X-ray beam. The scheme on top shows the film (disclike motive) location relative to the X-ray beam (arrows). In both cases the detector was placed as described in Figure 1b.

no signs of significant orientation (last column of Figure 8). These facts must be considered in order to interpret the values of the oriented fraction and of the Hermans orientation function represented in parts b and c of Figure 7, respectively. Here, it is detected that during crystallization the orientation in PBT tends to remain close to the zero level. The small initial value of the orientation function can be attributed to anisotropic microvoids oriented parallel to the flat surface. In spite of this initial orientation, the crystallization of the homopolymer proceeds isotropically as indicated by the values of Φ and f_2 (see Figure 7b,c). On the contrary, the PBT/0.1 wt % SWCNT

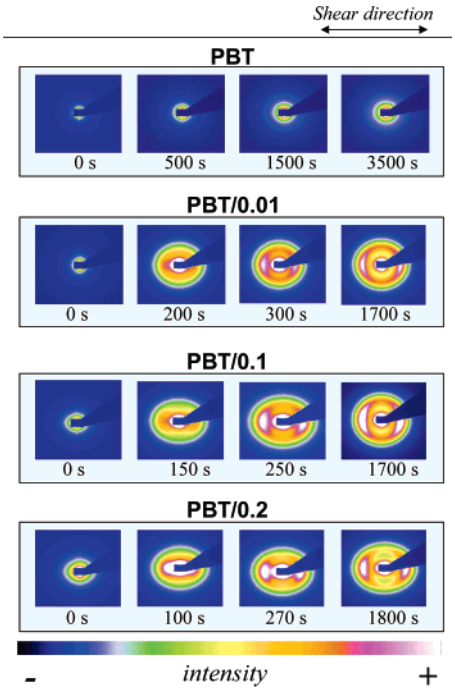

Figure 9. Series of two-dimensional SAXS patterns at specific crystallization times for PBT and the PBT/SWCNT nanocomposites at $T_c = 208$ °C after the application of a shear rate of 5 s^{-1} at $T = 240$ °C.

nanocomposite starts with negative value of Φ and f_2 to end up with positive ones. This indicates an initial contribution from scatterers oriented parallel to the film surface. SWCNT bundles lying essentially parallel to the flat surface of the sample may be the origin of this first contribution. It is worth mentioning that the initial values of Φ and f_2 for the nanocomposite are very different from those of the homopoymer(see Figure 7b,c). The final positive values of both Φ and f_2 indicate a contribution from scatterers perpendicularly oriented, which we attribute to the structure of the semicrystalline polymer.

3.3. Crystallization of PBT/SWCNT Nanocomposites after Step Shear. Figure 9 exhibits a series of SAXS patterns taken at specific crystallization times for PBT and the PBT/SWCNT nanocomposites at $T_c = 208$ °C after the application of a step shear at $T = 240$ °C (shear rate of 5 s^{-1}). The long spacing associated with the maximum in scattering intensity are smaller than those observed under quiescent conditions, as shown in Figure 6b. L values do not vary significantly with nanotube concentration but tend to decrease for low shear rates (Figure 6b). While PBT does not exhibit significant orientation features during crystallization, the sample with SWCNT shows a strong concentration of the SAXS intensity on the meridian. This is the case for all the nanocomposites investigated. Figure 10a shows the relative integrated intensity for a series of PBT/SWCNT nanocomposites during crystallization at $T = 208$ °C, after the application of a shear rate of 5 s^{-1}. Parts b and c of Figures 10 show the oriented fraction and Hermans orientation function, respectively, as a function of crystallization time. It is clear that the final oriented fraction increases with the amount of SWCNT. The development and evolution of the oriented fraction during the crystallization process appears to be complex and requires a deep examination of the Hermans orientation function (Figure 10c). The behavior of PBT does not differ significantly from that described under quiescent conditions. The sample with 0.01 wt % of SWCNT starts with negative values of the orientation function but soon evolves toward positive values for times $t > 50$ s. For the samples with higher SWCNT

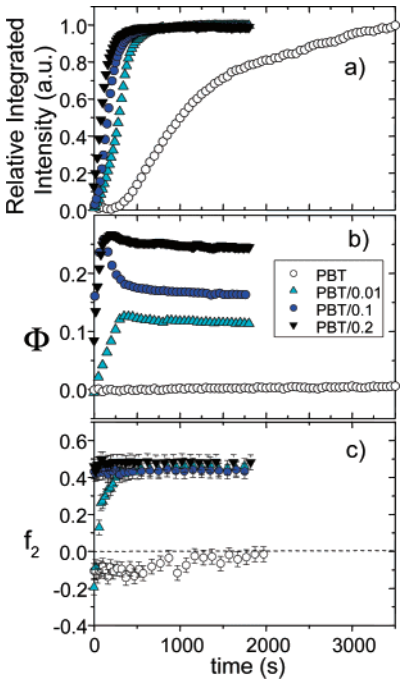

Figure 10. Variation of (a) SAXS relative integrated intensity, (b) oriented fraction, and (c) Hermans orientation factor for a series of SWCNT/PBT nanocomposites during crystallization at $T_c = 208$ °C after the application of a shear rate of 5 s^{-1} at $T = 240$ °C.

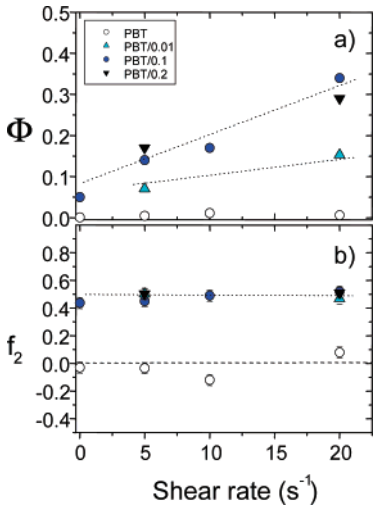

Figure 11. (a) Oriented fraction and (b) Hermans orientation function at the end of the crystallization process for the different samples and shear rates investigated.

concentration, positive f_2 values are always found along the crystallization process. In these cases, the orientation function does not vary during crystallization. These effects can be visualized by focusing on the initial and final SAXS patterns shown in Figure 9 for the different nanocomposites. Samples with 0 and 0.01 wt % of SWCNT exhibit, at the initial time, SAXS patterns with an excess of scattered intensity in the equatorial region, indicating an orientation of the scatterers in the direction of the shear. However, at the final crystallization times, the scattered intensity concentrates in the meridian part, indicating a predominant orientation of the scatterers perpendicular to the shear direction. Parts a and b of Figures 11 show the oriented fraction and the f_2 values, respectively, at the end of the crystallization process as a function of the shear rate for the different samples. Here, one sees that the oriented fraction achieved at the end of the crystallization process increases with

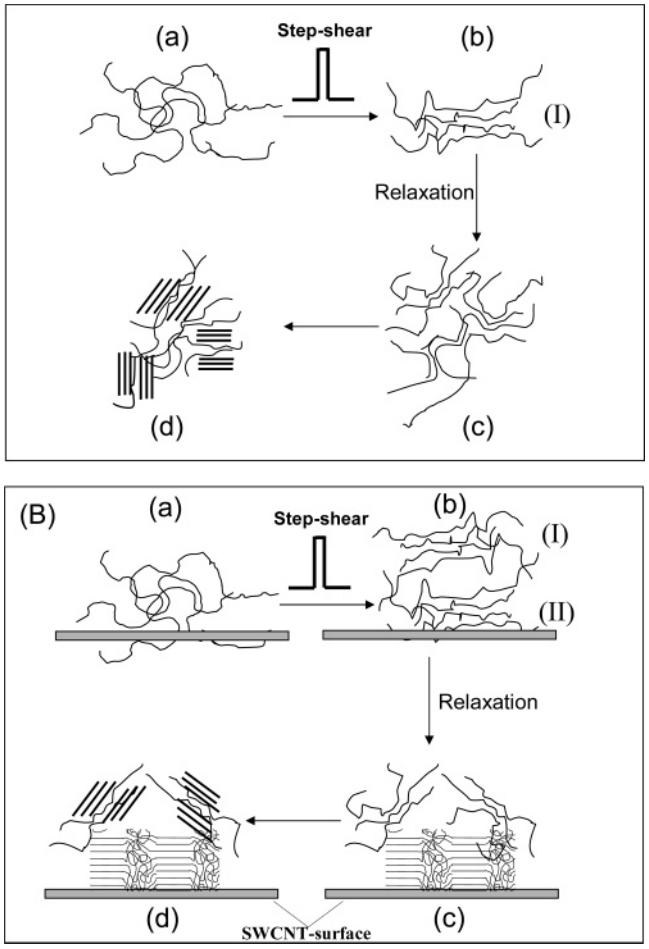

Figure 12. Schematic view of the morphological development during shear crystallization. (Top panel) PBT:[10] (a) random coil before shear, (b) shear-induced row nuclei, (c) formation of primary point nuclei due to relaxation of row nuclei, (d) isotropic crystal growth. (Bottom panel) PBT/SWCNT: (a) random coil before shear, (b) shear-induced row nuclei, (c) type I nuclei, far away from SWCNT surfaces, relax into primary point nuclei. Type II nuclei stabilize onto the SWCNT surfaces and originate anisotropic crystal growth on the SWCNT surface, (d) subsequent isotropic crystal growth originated by point nuclei.

the shear rate for the nanocomposites. However, the Hermans orientation function remains independent of the shear rate.

4. Discussion

The shear-induced crystallization of PBT has previously been described as being dominated by point nuclei.[10] As compared with polyolefins, polycondensation polymers like PBT do not reach the critical molecular weight above which, for a certain shear rate, molecular segments remain oriented long enough to template anisotropic crystallization.[8,23] Therefore, for crystallization at small supercooling conditions, the initial rodlike nuclei, which may appear as a consequence of shear, tend to relax, breaking into point nuclei. Because of this fact, little orientation is observed at the end of the crystallization process.[10] In our case, this effect is exemplified by the experiments performed at a shear rate of 10 s^{-1} (Figure 5). Here, it is seen that the oriented factor initially takes negative values tending at the end of crystallization to small and positive ones. The small and negative values of the initial Hermans orientation function can be interpreted as due to an initial orientation parallel to the shear of the polymer chains constituting the nuclei. Our results are in qualitative agreement with those ones reported for PBT.[10] Li et al. proposed a model like the one schematically represented

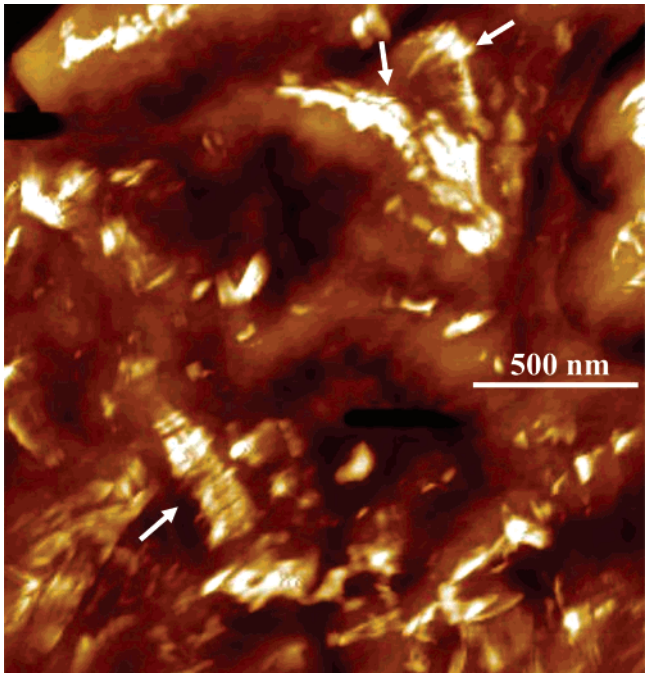

Figure 13. AFM phase image of the surface of a PBT/0.1 wt % SWCNT nanocomposite crystallized at $T_c = 208$ °C after the application of a shear rate of 10 s^{-1} at $T = 240$ °C. The arrows indicate probable shish-kebab-like motives.

in the top panel of Figure 12. Here, initial row nuclei formed after shear application evolved, due to relaxation, to point nuclei rendering to an essentially isotropic crystallization. This scenario for a poor oriented crystallization of PBT changes dramatically by the addition of modest quantities of SWCNT. Even under quiescent crystallization, the SWCNT template rather effectively oriented crystallization as revealed by the data presented in Figures 7 and 8. From the initial anisotropic SAXS pattern for the PBT/0.1 wt % SWCNT nanocomposite (Figure 8), a negative value of the Hermans orientation factor can be estimated (Figure 7). This fact can be attributed to the scattering of SWCNT located preferentially with their main axis parallel to the surface of the film. As crystallization proceeds, the Hermans factor evolves toward positive values because the scattered intensity tends to concentrate in the meridian. The oriented SAXS pattern for the same sample at the end of the quiescent crystallization (Figure 8) indicates that a certain amount of crystalline lamellae have grown perpendicular to the surface of the film. Accordingly, it is evident that SWCNT act as heterogeneous nuclei, providing surfaces over which oriented PBT crystals can grow. We can interpret that SWCNT bundles act as shish units in such a way that the nanocomposite structure resembles that of a shish kebab. As crystallization proceeds, those polymer crystals which are not in contact with the SWCNT surfaces exhibit little preference to remain oriented. As shown in Figure 6, shear affects significantly both the half time of crystallization and the long spacing of PBT. However, it has a minor effect on these two magnitudes in the case of the nanocomposites. Moreover, for the nanocomposites, the Hermans orientation function results are practically unaffected by the shear conditions investigated (Figure 11). This indicates that the presence of SWCNT is the dominant factor in the final level of orientation rather than the shearing conditions. Nevertheless, the final fraction of oriented crystalline material in the PBT/SWCNT nanocomposites increases significantly with the shear rate

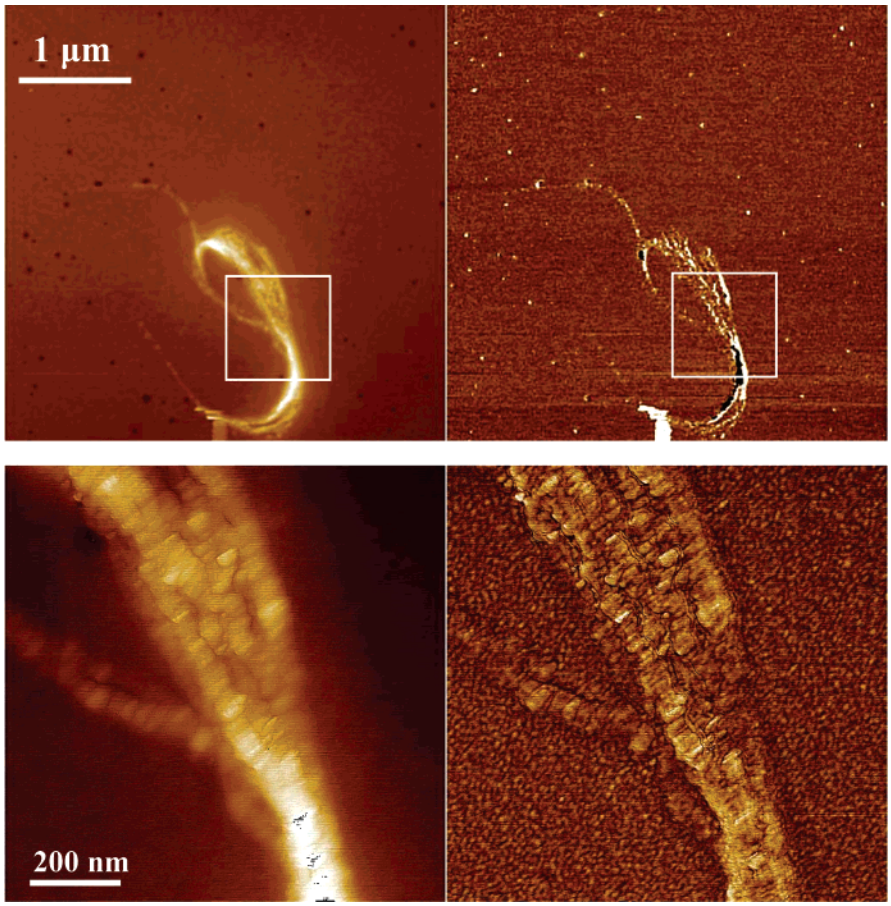

Figure 14. AFM images of a spin-coated PBT/0.2 wt % SWCNT nanocomposite. Upper and lower panels are different magnifications indicated by the scale bars. Left and right pictures correspond to the height and phase images, respectively.

(Figure 11). On the basis of the model of Li et al.,[10] we propose that the presence of SWCNT modifies the crystallization process as schematically described in the bottom panel of Figure 12. After shear, initial row nuclei develop in the polymer melt. Nuclei far away from the SWCNT surface can relax but those close to these surfaces do not. Consequently, SWCNT provide surfaces which stabilize nuclei, enhancing oriented crystallization with crystalline lamellae growing perpendicular to the SWCNT surface. This effect is expected to operate in addition to the usual quiescent nucleation effect of SWCNT. As crystallization proceeds, polymer material located far away from SWCNT surfaces grows without any preferred orientation and this provokes the decay of the oriented fraction in the final stages of crystallization, as observed in Figure 10b. Shish-kebab structures induced by SWCNT have been reported for nanocomposites based on polyethylene[13,15,24] and its oligomers.[25] A similar morphology has also been reported in polyethylene/sorbitol composites.[26] On the basis of SAXS experiments, the existence of shish-kebab microstructure was proposed for injection molded samples of PBT/SWCNT.[14,17] Ex situ investigation of the surface of some sheared samples by AFM shows the presence of shish-kebab like motives as those illustrated by arrows in Figure 13 for a PBT/0.1 wt % SWCNT nanocomposite crystallized at $T_c = 208$ °C after the application of a shear rate of 10 s^{-1} at $T = 240$ °C. Additional AFM investigations were performed on spin coated samples. Figure 14 shows two AFM images with different magnification of a spin-coated PBT/0.2 wt % SWCNT nanocomposite. Here, the presence of a characteristic SWCNT bundle is clearly seen in Figure 14 for the lower resolution. A magnification of one of the bundle branches, Figure 14 bottom panel, indicates the formation of crystalline blocks in a shish-kebab fashion along the main axis of the SWCNT bundle. It is clear that the preparation conditions of the specimen for AFM are very different from those of the sheared samples. However, the AFM results support the existence of shish-kebab-like structures in PBT/SWCNT nanocomposites.

5. Conclusions

The influence of single wall carbon nanotubes and shear on the templating of polymer crystallization has been studied in PBT/SWCNT nanocomposites. The main conclusions can be itemized as follows: (1) SWCNT bundles tend to template crystallizing polymer lamellae to grow perpendicularly to the SWCNT surfaces in a shish-kebab-like fashion. This effect occurs under both quiescent and sheared melt conditions for the experimental conditions investigated. For the nanocomposites, shear has a minor effect on the crystallization kinetics and on the orientation level reached after crystallization. (2) However, shear rate controls the fraction of oriented material which increases significantly with shear rate. It is proposed that the effect of SWCNT is to counterbalance nuclei relaxation by providing surfaces which stabilize some of them.

Our experiments emphasize the complexity of the crystalline structures which may appear in SWCNT nanocomposites when processed under the combination of complex force fields and temperature gradients.

Acknowledgment. The authors thank the MEC (Grant MAT2005-01768), Spain, for their generous financial support for this investigation. M.C.G.-G. and A.N. are also grateful to the Ramón y Cajal Program for the support of this research. J.J.H thanks the Spanish Ministry for Science and Education (MEC) for the tenure of a fellowship. The assistance of S.S. Funari during measurement time at Hasylab, Hamburg (Germany) is also acknowledged. We thank M. Kwiatkowska and Z. Rosłaniec for sample preparation.

References and Notes

(1) Iijima, S. *Nature* **1991**, *354*, 56.
(2) Terrones, M. *Annu. Rev. Mater. Res.* **2003**, *33*, 419.
(3) Dresselhaus, M. S.; Eklund, P. C. *Adv. Phys.* **2000**, *49*, 705.
(4) *Carbon Nanotubes: Properties and Applications*; O'Connell, J. O., Ed. Taylor & Francis: Boca Raton, FL, 2006.
(5) Moniruzzaman, M.; Winey, K. I. *Macromolecules* **2006**, *39*, 5194.
(6) Vaia, R. A.; Wagner, H. D. *Mater. Today* **2004**, *November*, 32.
(7) Thess, A.; Lee, R.; Nikolaev, P.; Dai, H.; Petit, P.; Robert, J.; Xu, C.; Hee Lee, Y.; Gon Kim, S.; Rinzler, A. G.; Colbert, D. T.; Scuseria, G. E.; Tomanek, D.; Fischer, J. E.; Smalley, R. E. *Science* **1996**, *273*, 483.
(8) Somani, R. H.; Hsiao, B. S.; Nogales, A.; Srinivas, S.; Tsou, A. H.; Sics, I.; Balta-Calleja, F. J.; Ezquerra, T. A. *Macromolecules* **2000**, *33*, 9385.
(9) Seki, M.; Thurman, D. W.; Oberhauser, J. P.; Kornfield, J. A. *Macromolecules* **2002**, *35*, 2583.
(10) Li, L.; de Jeu, W. H. *Macromolecules* **2004**, *37*, 5646.
(11) Heeley, E. L.; Fernyhough, C. M.; Graham, R. S.; Olmsted, P. D.; Inkson, N. J.; Embery, J.; Groves, D. J.; McLeish, T. C. B.; Morgovan, A. C.; Meneau, F.; Bras, W.; Ryan, A. J. *Macromolecules* **2006**, *39*, 5058.
(12) Bhattacharyya, A. R.; Sreekumar, T. V.; Liu, T.; Kumar, S.; Ericson, L. M.; Hauge, R. H.; Smalley, R. E. *Polymer* **2003**, *44*, 2373.
(13) Li, C. Y.; Li, L.; Cai, W.; Kodjie, S. L.; Tenneti, K. K. *Adv. Mater.* **2005**, *17*, 1198.
(14) García-Gutiérrez, M. C.; Nogales, A.; Rueda, D. R.; Domingo, C.; García-Ramos, J. V.; Broza, G.; Roslaniec, Z.; Schulte, K.; Davies, R. J.; Ezquerra, T. A. *Polymer* **2006**, *47*, 341.
(15) Haggenmueller, R.; Fischer, J. E.; Winey, K. I. *Macromolecules* **2006**, *39*, 2964.
(16) Minus, M. L.; Chae, H. G.; Kumar, S. *Polymer* **2006**, *47*, 3705.
(17) García-Gutiérrez, M. C.; Nogales, A.; Rueda, D. R.; Domingo, C.; García-Ramos, J. V.; Broza, G.; Roslaniec, Z.; Schulte, K.; Ezquerra, T. A. *Compos. Sci. Technol.* **2007**, *67*, 798.
(18) Panine, P.; Gradzielski, M.; Narayanan, T. *Rev. Sci. Instrum.* **2003**, *74*, 2451.
(19) Broza, G.; Kwiatkowska, M.; Rosłaniec, Z.; Schulte, K. *Polymer* **2005**, *46*, 5860.
(20) Nogales, A.; Broza, G.; Rosłaniec, Z.; Schulte, K.; Sics, I.; Hsiao, B. S.; Sanz, A.; García-Gutiérrez, M. C.; Rueda, D. R.; Domingo, C.; Ezquerra, T. A. *Macromolecules* **2004**, *37*, 7669.
(21) Hwang, W. R.; Peters, G. W. M.; Hulse, M. A.; Meijer, H. E. H. *Macromolecules* **2006**, *39*, 8389.
(22) Prasad, A.; Shroff, R.; Rane, S.; Beaucage, G. *Polymer* **2001**, *42*, 3103.
(23) Keller, A; Kolnaar, H. W. *Flow Induced Orientation and Structure Formation In Processing of Polymers*; Meijer, H. E. H., Ed.; VCH: New York, 1997; p 189.
(24) Zhang, Q. H.; Lippits, D. R.; Rastogi, S. *Macromolecules* **2006**, *39*, 658.
(25) Li, L.; Yang, Y.; Yang, G.; Chen, X.; Hsiao, B. S.; Chu, B.; Spanier, J. E.; Li, C. Y. *Nano Lett.* **2006**, *6*, 1007.
(26) Nogales, A.; Olley, R. H.; Mitchell, G. R. *Macromol. Rapid Commun.* **2003**, *24*, 496.

MA0713512